Heat and moisture insulation by means of air curtains. Application to refrigerated chambers

H. Giráldez[a], C.D. Pérez Segarra[a], C. Oliet[a], A. Oliva[a,*]

[a]*Heat and Mass Transfer Technological Centre (CTTC), Universitat Politècnica de Catalunya - BarcelonaTech (UPC) ETSEIAT, Colom 11, 08222 Terrassa (Barcelona), Spain.*

Abstract

The present study is devoted to the determination of the efficiency of air curtain units (ACUs) applied to heat and moisture insulation of refrigerated chambers. A detailed study of the fluid dynamics and heat and mass transfer of the ACU in the refrigerated space and the external ambient is carried out by means of large eddy simulations (LES). The heat and moisture entrainment through the doorway and their transport inside the inner space are fully described. Three different configurations are studied: non-recirculating, recirculating and twin-jet air curtains. The condensation produced in the cool walls of the refrigerated space is evaluated considering the warm humid air from the ambient which penetrates inside the chamber through the doorway. The influence of both the discharge velocities and the discharge angles on the sealing capabilities of the three different tested ACU configurations is determined.

Keywords: air curtain, recirculating, twin-jet, thermal energy efficiency, condensation, LES turbulence model

*Corresponding author. Tel: +34 93 739 8192; fax: +34 93 739 8101
Email address: cttc@cttc.upc.edu (A. Oliva)

Nomenclature

C_w	turbulence model constant [-]
c_p	specific heat at constant pressure $[J\ kg^{-1}\ K^{-1}]$
D_v	diffusivity of water vapour in air $[m^2\ s^{-1}]$
E_{ff}	air curtain sealing efficiency [-]
$\dot{G}$	mass flux rate $[kg\ m^{-2}\ s^{-1}]$
g	gravity acceleration $[m\ s^{-2}]$
L_v	latent heat of vapourisation $[J\ kg^{-1}]$
Pr	Prandtl number, $Pr = \mu\ c_p/\lambda$ [-]
RH	Relative humidity [-]
$\boldsymbol{S}$	rate of stress tensor $[s^{-1}]$
$\boldsymbol{\mathcal{S}}$	traceless symmetric part of square of $\boldsymbol{\gamma}$ $[s^{-2}]$
Sc	Schmidt number, $Sc = \nu/D_v$ [-]
$\mathbf{u}$	velocity vector with components (u,v,w) $[m\ s^{-1}]$
Y_v	mass fraction of water vapour[-]
x, y, z	Cartesian coordinates $[m]$

Greek symbols

α	thermal diffusivity, $\alpha = \lambda/\rho/c_p$ $[m^2\ s^{-1}]$
$\boldsymbol{\gamma}$	velocity gradient tensor $[s^{-1}]$
Δ	length scale of the filter $[m]$
Δl	characteristic length of the control volume $[m]$
Δt	time step $[s]$

$\boldsymbol{\delta}$	unit tensor [-]
θ	nozzle discharge angle [°]
λ	thermal conductivity [$W\ m^{-1}\ K^{-1}$]
μ	dynamic viscosity [$kg\ s^{-1}\ m^{-1}$]
ν	kinematic viscosity [$m^2\ s^{-1}$]
ν_e	kinematic eddy viscosity [$m^2\ s^{-1}$]
ρ	density [$kg\ m^{-3}$]
$\boldsymbol{\tau}$	Reynolds stress tensor [$m^2\ s^{-2}$]
$\overline{\phi}$	filtered variable (ϕ=**u**, p, T, Y_v,...)

Subscripts

da	dry air
δ	liquid-gas interface
e	effective
g	gas phase
t	turbulent
v	water vapour
ω	liquid water

1. Introduction

An air curtain unit (ACU) is a device which produces a plane impinging jet acting as an ambient separator. The application of ACUs in the refrigera-

tion and HVAC fields implies the need for determining the efficiency of these devices to avoid both the heat and moisture entrainment in the protected spaces. The jet produced by the ACU and its sealing capability strongly depend on the difference of pressure and/or temperature between the inner (protected) and outer (ambient) spaces and the wind effect. The efficiency of ACUs has been studied by several authors since the 60s.

The studies of Hetsroni [1] and Hayes [2] are the first attempts to characterise ACUs by means of simplified models. Later Siren [3] [4] introduced a semi-analytical method which allows a more accurate dimensioning of these devices. More recently Giraldez et al. [5] proposed an improved semi-analytical methodology that takes into account deviations in the jet trajectory that can produce additional losses.

More advanced strategies using CFD (Computational Fluid Dynamics) techniques have been extensively applied. Foster et al. [6] use a 2D CFD model to evaluate the effectiveness and optimum jet velocity for a plane jet air curtain. They studied the importance of the shape of the jet and the influence on the air curtain effectiveness of the jet velocity and door-open duration. However, the results of the 2D analysis were not satisfactory and the necessity of 3D simulations was pointed out. Subsequently, these authors [7] presented a 3D simulation where the influence of the stack pressures on the deflection of the lateral ends of the air curtain is analysed.

Different CFD studies have been carried out on open vertical display cabinets where air curtains separate the protected refrigerated space from the exterior. D'Agaro et al. [8] showed that secondary vortices at the side walls provide the most important mechanism for air entrainment. Compar-

ison with experimental results showed that 3D computations are required to properly describe the air flow, a 2D simulation being inadequate for such configurations. Cortella et al. [9] implemented a 2D finite element code based on the stream function-vorticity formulation, and LES turbulence modelling for the analysis of air flow and temperature distributions (fully 3D LES modelling was used by the authors in the above mentioned paper [5]). Valkeapää and Siren [10] studied the thermal energy efficiency of ACUs, comparing both recirculating and non-recirculating installations. They apply the semi-analytical approach developed by Siren [3] to study an upward blowing ACU. They found that the upper limit for the tightness of recirculating installations is about 80%.

Hammond at al. [11] proposed a design guide for cabinet designers based on experimental work and CFD analysis using a 2D model. Navaz et al. [12] focused the attention on three important parameters which condition the flow entrainment in ACUs: turbulence intensity, Reynolds number and velocity profile at the discharge, and their effect on the development of turbulence and mixing. Marinetti et al. [13] simulate the 3D isothermal air flow inside cooling ducts of horizontal open type cabinet. They showed the capability of the model to predict the main features of the flow field.

None of the above mentioned papers consider the vapor transport from the humid air. Furthermore, all of them (except the papers already mentioned by Cortella et al. [9], and the one by the authors [5]) use commercial CFD codes and standard two equation RANS modelling (in general k-ϵ models).

Turbulence modelling using RANS (Reynolds Averaged Navier Stokes) approach is based on the time average Navier Stokes equations. As it is well

known, time averaging generates new unknowns (the turbulent Reynolds stresses and heat fluxes), which have to be modelled. This is a formidable task because these terms are highly anisotropic and involve all the scales of the turbulent flow. A wide variety of models have been proposed the above mentioned two-equation models being the most popular. The accuracy of the simulations is very dependent on the turbulence model and the selection of the most appropriate one for a specific application is crucial. Jaramillo et al. [14] analysed air curtain devices applied to refrigerated chambers. Their studies showed that numerical results are strongly dependent on the different turbulence models tested (algebraic Reynolds stress and linear and non-linear k-ϵ and k-ω RANS models).

In this sense, LES (Large Eddy Simulation) is a much more powerful approach. The largest scales of the turbulent flow, which are anisotropic, unsteady and 3D, are solved in detail while only the smallest scales (the so called subgrid scales) are modelled. Even though LES is computationally more demanding than RANS, their simulation capabilities are much higher.

The main objective of this paper is to present an analysis of the efficiency of vertical downward blowing air curtains applied to refrigerated rooms, considering both the energy and water vapour entrainment from the external warm and humid ambient air. The simulation is fully 3D and the LES approach is applied.

Velocity, pressure and temperature fields are calculated together with the water vapour concentration, which is transported both by diffusion and convection through the air curtain, and into the inner or refrigerated space. Once the moisture enters the refrigerated space, water condensation on the

cold walls can be produced. Both the thermal energy and vapour entrainment efficiencies of the installation are calculated by comparing the current entrainments with the ones when the ACU is turned off.

The paper is divided into three main sections. In the first one, the mathematical model and numerical methodology are detailed. In the second section, computational results are compared with experimental data obtained by the authors and from published data in the literature. After demonstrating the capabilities of the simulation procedure, the third section shows a parametric study where three different ACU configurations (non-recirculating single jet, twin jets and recirculating ACU) are tested under different working conditions. The optimum discharge velocity and discharge angle for minimizing the entrainment produced by the temperature and moisture differences between the inner space (refrigerated room) and the outside (external ambient) are evaluated.

2. Mathematical formulation and numerical model

The air jet produced by an ACU is fully turbulent. In this section, its mathematical description based on the filtered three-dimensional Navier-Stokes equations and using LES turbulence models are described. Important aspects related to the boundary conditions and the numerical resolution are also presented.

2.1. Governing equations

Assuming Newtonian incompressible air flow behaviour and constant viscosity, the filtered equations of mass and momentum can be written as follows:

$$\nabla \cdot \bar{\mathbf{u}} = 0 \tag{1}$$

$$\frac{\partial \bar{\mathbf{u}}}{\partial t} + \nabla \left(\bar{\mathbf{u}} \bar{\mathbf{u}} \right) + \frac{1}{\rho_o} \nabla \bar{p} - \nu \nabla^2 \bar{\mathbf{u}} - \frac{\rho \mathbf{g}}{\rho_o} = \nabla \cdot \boldsymbol{\tau} \tag{2}$$

where $\bar{\mathbf{u}}$ and $\bar{p}$ represent the filtered velocity and pressure fields. The Boussinesq hypothesis is applied, which assumes constant density everywhere (ρ_o is evaluated at reference conditions) except density variations due to temperature changes in the buoyancy term. The right-hand side of the momentum equations stands for the turbulent scales which are smaller than the mesh size (subgrid scales).

$$\boldsymbol{\tau} = \bar{\mathbf{u}} \bar{\mathbf{u}} - \overline{\mathbf{u}\mathbf{u}} \tag{3}$$

These subgrid scales have been modelled using an eddy viscosity approach,

$$\boldsymbol{\tau} = \frac{1}{3} \boldsymbol{\tau} : \boldsymbol{\delta} + 2 \nu_e \overline{\mathbf{S}} \tag{4}$$

$$\overline{\mathbf{S}} = \frac{1}{2} \left[\nabla \bar{\mathbf{u}} + \nabla \bar{\mathbf{u}}^T \right] \tag{5}$$

where $\bar{\mathbf{S}}$ is the filtered rate of stress tensor. In this study, the Wall Adapting Local Eddy viscosity (WALE) model [16] is employed. According to this model, the expression for the eddy viscosity is given by

$$\nu_e = \left(C_w \Delta \right)^2 \frac{\left(\overline{\boldsymbol{\mathcal{S}}} : \overline{\boldsymbol{\mathcal{S}}} \right)^{3/2}}{\left(\overline{\mathbf{S}} : \overline{\mathbf{S}} \right)^{5/2} + \left(\overline{\boldsymbol{\mathcal{S}}} : \overline{\boldsymbol{\mathcal{S}}} \right)^{5/4}} \tag{6}$$

where Δ is the length scale of the filter, C_w is the turbulence model constant ($C_w = 0.325$), and $\boldsymbol{\mathcal{S}}$ is the traceless symmetric part of the square of the velocity gradient. In tensor notation:

$$\overline{S_{ij}} = \frac{1}{2}\left(\overline{\gamma}_{ij}^2 + \overline{\gamma}_{ji}^2\right) - \frac{1}{3}\delta_{ij}\overline{\gamma}_{kk}^2 \tag{7}$$

$$\bar{\gamma}_{ij} = \frac{\delta \bar{u}_i}{\delta x_j} \tag{8}$$

The energy equation governs the temperature distribution in the whole domain:

$$\frac{\partial \bar{T}}{\partial t} + \bar{\boldsymbol{u}} \cdot \nabla \bar{T} = \nabla \cdot \left[\left(\frac{\nu}{Pr} + \frac{\nu_e}{Pr_t}\right)\nabla \bar{T}\right] \tag{9}$$

where Pr is the Prandtl number and Pr_t is the turbulent Prandtl number. The Prandtl number is a function of species mass fraction. The moisture affects the local Prandtl number due to the variable thermophysical properties of the air-water mixture, that have been calculated according to Fessler [17].

For the turbulent Prandtl number, the usual value of 0.4 has been taken [18],[19].

The water vapour concentration in humid air can be described by its transport equation:

$$\frac{\partial \bar{Y}_v}{\partial t} + \bar{\boldsymbol{u}} \cdot \nabla \bar{Y}_v = \nabla \cdot \left[\left(\frac{\nu}{Sc} + \frac{\nu_e}{Sc_t}\right)\nabla \bar{Y}_v\right] \tag{10}$$

where Y_v is the water vapour concentration, and Sc and Sc_t are the Schmidt number and the turbulent Schmidt number, respectively.

For the turbulent Schmidt number a value of 0.4 has been taken based on the work of Launder [18] and Reynolds [19].

2.2. Boundary Conditions

In refrigerated chambers two main zones can be defined: the chamber itself and the external ambient. For the latter, and far from the air curtain, two situations can be considered: outflow and inflow zones.

At the outflow boundaries the external pressure is imposed, and the gradients in the normal direction of the temperature and vapour concentration are set to zero. At the inflow zones, fixed values of the different variables are given (the ones corresponding to these external boundaries).

At the air curtain discharge, the three velocity components are given, which depend on the ACU, while the temperature and vapour concentration are prescribed according to their upstream values (the ones at the inlet of the ACU) calculated from the simulation of the refrigerated space.

Inside the refrigerated chamber, the solid walls can be treated as adiabatic or isothermal surfaces. In these walls, non-slip conditions have been assumed. Condensation of the water vapour contained in the humid air can occur on the cold surfaces if their temperature is below the corresponding dew point temperature.

Therefore, when the dew point temperature is reached, the wall acts as a sink for the water vapour concentration. The water film produced by the condensed water is not considered in the simulation (it is assumed that the liquid film is completely eliminated from the chamber).

In the case of condensation, the following boundary conditions are given. At the liquid/humid air interface, the dry air mass flow rate must be zero, $\dot{G}_{da,\delta} = 0$. Therefore, the total mass transfer (diffusion plus convection) of water vapour at the interface is

$$\dot{G}_{v,\delta} = -\frac{\rho D_v}{(1 - Y_{v,\delta})} \left(\frac{\partial Y_v}{\partial n} \right)_\delta \tag{11}$$

where n represents the normal direction to the wall, $Y_{v,\delta}$ is the vapour mass fraction at the interface ($n = \delta$), and D_v is the diffusion coefficient of water vapour in air.

Furthermore, $Y_{v,\delta}$ corresponds to saturation conditions at the interface. Finally, continuity of shear stresses and energy fluxes gives:

$$\mu_l \left(\frac{\partial v_w}{\partial n} \right)_\delta = \mu \left(\frac{\partial v}{\partial n} \right)_\delta \tag{12}$$

$$-\lambda_l \left(\frac{\partial T_w}{\partial n} \right)_\delta = -\lambda \left(\frac{\partial T}{\partial n} \right)_\delta + L_v \dot{G}_{v,\delta} \tag{13}$$

where L_v represents the liquid-vapour latent heat of water, μ_l and λ_l are the dynamic viscosity and thermal conductivity of liquid water, and μ and λ represent the properties of humid air.

2.3. Numerical model

All the simulations are carried out using the CFD & HT code Termofluids [20], which is a parallel object-oriented code for solving industrial flows. In Termofluids, the governing equations are discretized on a collocated unstructured grid arrangement, and using second-order spectro-consistent schemes [21]. Such discretization preserves the symmetry properties of the continuous differential operators, and ensures both stability and conservation of the global kinetic-energy balance on any grid. For the temporal discretization, a two-step linear explicit scheme on a fractional-step method has been

used for the convective and diffusive terms [22], while for the pressure gradient term an implicit first-order scheme is employed. For the determination of the time step the Courant-Friedrichs-Lewy (CFL) condition has been employed:

$$\Delta t = min(\Delta t_{conv}, \Delta t_{visc}, \Delta t_{cond}, \Delta t_{vap}) \tag{14}$$

where,

$$\Delta t_{conv} = 0.25\frac{\Delta l}{u}, \quad \Delta t_{visc} = 0.25\frac{\Delta l^2}{\nu}, \quad \Delta t_{cond} = 0.2\frac{\Delta l^2}{\alpha}, \quad \Delta t_{vap} = 0.1\frac{\Delta l^2}{D_v} \tag{15}$$

where Δl is a characteristic length of the control volume (cubic root of its volume).

This methodology has been successfully applied in many flows similar to the ones presented in ACUs (e.g. turbulent plane jets and flows bluff bodies with massive separation [23], [24]), and in different cases of natural and mixed convection in enclosures [25], [26].

3. Comparison of computational results with experimental data

For the simulation of the refrigerating chamber, the model considers the transport of water vapour from the humid air which enters the protected space through the doorway. In order to check the capabilities of the mathematical model presented in the previous section, three different situations have been considered:

- Plane air jet with stagnant external ambient conditions.

- Surface evaporation of water vapour in presence of air on a horizontal pool.
- Evaporation from a water film on a vertical wall.

The second and third cases have been specifically chosen to analyse the mass diffusion effect of humid air produced by the water vapour transport from the liquid surface.

3.1. Case 1: Plane air jet with stagnant external ambient conditions

Before the coupled simulations of moisture and thermal energy entrainment are carried out, the dynamics of the plane air jet produced by an ACU has been studied both numerically and experimentally.

The experimental setup was described by the authors in [28]. Experimental measurement is carried out following the standard procedure for air curtains characterization according to ANSI/AMCA [27].

The studies showed the mean core velocity evolution of a plane air jet, which presents different regions, progressively reducing the maximum velocity and spreading the air jet in the spanwise direction. This effect diminishes its capability to act as a separator. It was seen that low discharge velocities produce weak air jets, which cannot avoid the entrainment of external air. As an example, Fig.1(a) shows a LES simulation where the typical deflection and air entrainment produced by external forces acting against the weak air jet can be seen. In the case of an air curtain with a high discharge velocity (see Fig.1(b)), the external forces cause a lower deflection and do not break the jet.

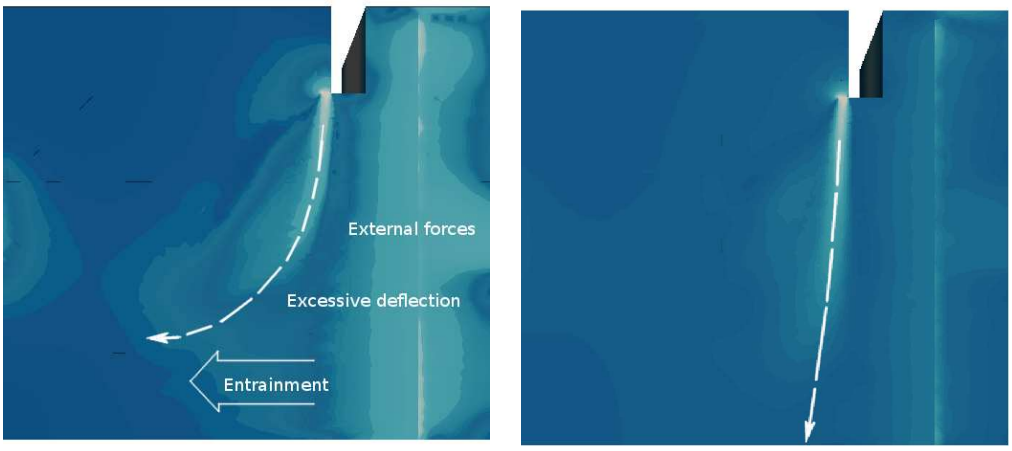

(a) (b)

Figure 1: Case 1: Trajectories of air jets produced by an ACU. (a)Air jet which presents an excessive deflection due to external forces. (b)Air jet which totally seals a refrigerated chamber.

The results already presented by the authors (see [5]) show that the air jet behaviour predicted by the mathematical models employed here (LES with WALE model) agrees with the experimental measurements. In that previous work, the authors carried out experimental measurements at different distances from the ACU discharge and compared the obtained downstream core velocity evolution with the results obtained numerically. The experimental measurements showed some dispersion in every distance. For instance, one meter downstream of the ACU discharge section the numerical results overestimate the mean core velocity with an error of approximately 8 per cent (see [5]). The mean core velocity determined numerically was found inside the experimental uncertainty range (between $\pm 1 m/s$ relative to the mean core velocity).

3.2. Case 2: Surface evaporation of water vapour in presence of air flow over a horizontal pool

In order to check the accuracy of the mathematical model considering mass transfer diffusion, the same case proposed by Talukdar et al. [29] is considered. It consists of a water pool partially evaporating and condensing with a parallel dry air stream flowing above it. As expected, the initially dry air stream progressively increases its water mass fraction as it flows through the domain. The objective of the study is the comparison of the calculated velocities, temperatures and water vapour concentrations of the air flow with the experimental data given in [29].

The geometry of the system (see Fig.2) is a horizontal 3D rectangular duct with a water pan centred on the bottom of the channel. All the other surfaces of the channel (lateral and top walls) are considered adiabatic.

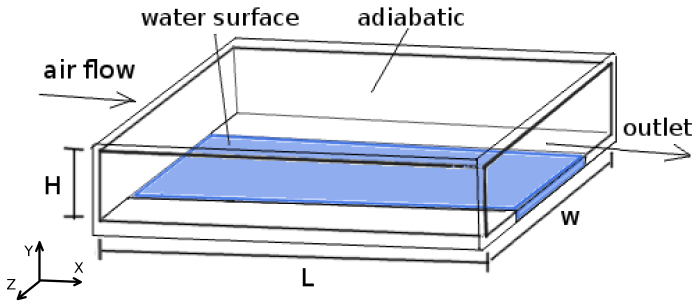

Figure 2: Case 2: Scheme of the horizontal pool case.

For the air flow, and according to [29], a fully developed laminar velocity profile of air is assumed at the entrance with a constant temperature and relative humidity. The flow is assumed to be steady.

At the bottom wall (y = 0), the water is at rest.

The simulation was carried out using a structured mesh of 250.000 control volumes. The mesh is progressively concentrated near the solid walls of the channel and near the water surface in order to accurately capture the higher gradients in these regions.

Ten different situations are simulated, which present different boundary conditions at the entrance of the channel ($x = 0$). Fig.3 shows the values of temperature and relative humidity of the air flow at the exit section of the domain ($x = L$).

In all the situations a good agreement between the experimental measurements and the calculations presented here can be observed. The maximum discrepancies present an error below 5 per cent.

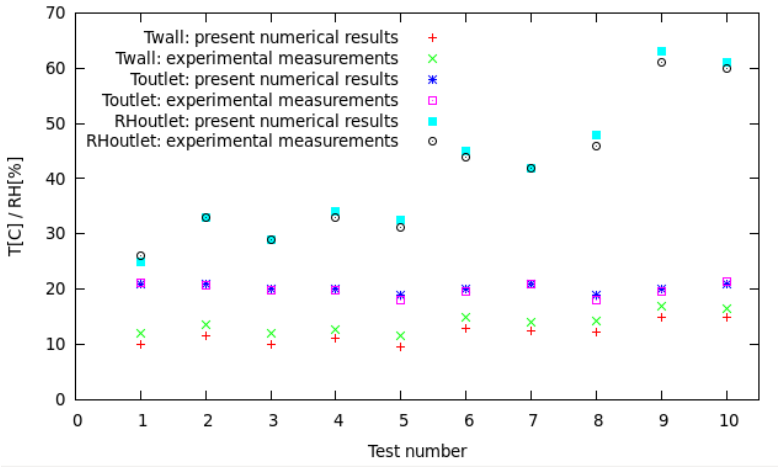

Figure 3: Case 2: Air flow film temperature and relative humidity at the duct outlet. Comparison of numerical results and experimental data (from [29]).

3.3. Case 3: Evaporation from a water film in a vertical wall

In the cool surfaces of a refrigerating space, condensation of the water vapour can create a liquid film. Once the film is formed, the flow of water is moving down by the gravity effect. The liquid film is partially evaporated to the surrounding air. This third case, referred to falling film, describes this transport phenomena.

Experimental data by Jabrallah et al. [30] have been used to test the mathematical model. A scheme of the case is shown in Fig.4.

As can be seen, the liquid film falls vertically attached to the wall under the gravity effect and suffers evaporation which diminishes its total mass flow.

A comparison of the numerically predicted and experimentally obtained water film temperature distributions in the horizontal middle section (y=H/2.0)

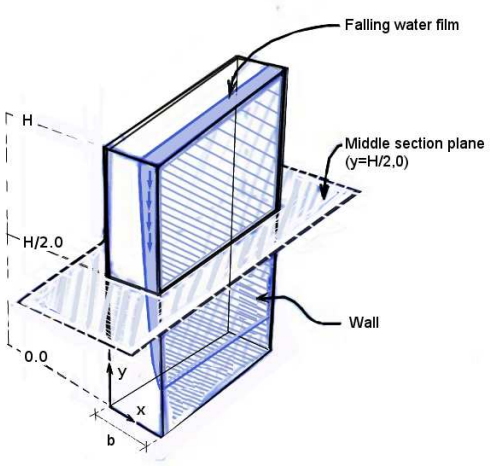

Figure 4: Case 3: Scheme of the falling film on a vertical wall.

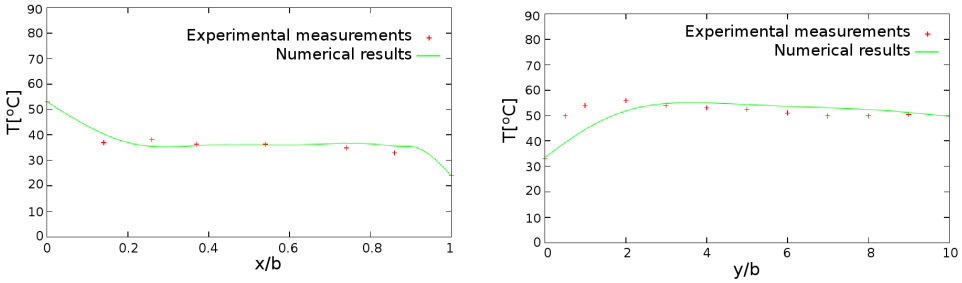

(a) (b)

Figure 5: Case 3: Falling film. Comparison of the numerical results and experimental data (from [30]). (a)Temperature distribution in the horizontal middle section (x, y=H/2, z=W/2). (b)Temperature distribution along the wall.

and along the wall are presented. The film temperature, is calculated as the mean value between the temperature of the wall and the gas-liquid interface temperature.

The numerical calculations slightly overestimate the temperature in the central region of the wall (see Fig.5(b)), but discrepancies with experimental data are lower than 2%. In any of the tested cases, maximum discrepancies have been lower than 10%.

Even though this physical process is just the opposite in a refrigerating space (condensation instead of evaporation), the mathematical formulation is exactly the same and the obtained numerical results in the two previous validation tests (pool within a rectangular duct [29] and falling film in a cavity [30]) confirm the capabilities of the mathematical model developed.

4. Numerical study of air curtain in refrigerating spaces under condensation conditions

A detailed analysis of air curtains considering both heat and moisture transport is presented in this section. The heat and moisture entrainment produced through the doorway are determined for different configurations and working conditions. The efficiency of the ACU is calculated by comparison with the situation where the ACU is turned off. The water vapour transported and condensed in the refrigerated space is also evaluated.

4.1. Problem definition and mesh generation

Three configurations have been studied: non-recirculating (standard case), recirculating and twin-jets ACU. The geometry of the physical domain consists of two adjacent spaces, the refrigerated room and the external ambient,

connected by an opened door of 1.0 m wide and 2.0 m high (see Fig.6(a)). The ACU is installed on the top of the doorway opening. The discharge air curtain nozzle, on the lower face of the device, has a width of 6 cm and a length of 1.0 m, covering the whole door width. In the recirculating configuration, the ground has a receptor vent that allows the air flow to return to the ACU suction by means of ducts which are located inside the walls (see Fig. 7 and Fig. 8). In the twin-jets configuration, the ACU has two jets of 3 cm wide with a 3 cm separation between them. As a rule, positive discharge angles are towards the inside of the refrigerated chamber, while the negative angles are towards the outside.

The size of the external (ambient) space must be large enough to have no interaction on the air curtain. Different sizes have been tested. Calculations confirm that the influence of the farthest external (relative to the air curtain) boundary is negligible.

An unstructured mesh is employed. The mesh has approximately 400,000 control volumes, most of them in the region which covers the air jet (see Fig.6(b)). A high mesh concentration near the solid walls is employed to correctly solve the boundary layer.

In order to check the quality of the mesh, three different meshes have been studied: a coarse mesh of 0.15 million control volumes (MCV), a middle mesh of 0.40 MCV and a fine mesh of 1 MCV. Results are presented in Fig. 9, where the water entrainment time evolution is given. As can be seen, the middle and fine meshes give very similar results, with maximum discrepancies lower than 2%. Similar results were obtained for the thermal energy entrainment. Therefore, the middle mesh (0.40 MCV) has been chosen to carry out the

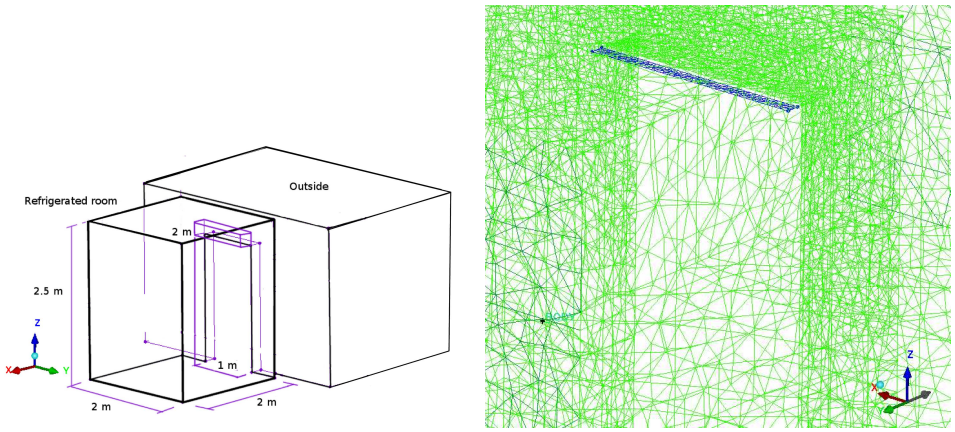

(a) (b)

Figure 6: (a) Geometry of the calculation domain and (b) Detail of the computational mesh in the doorway.

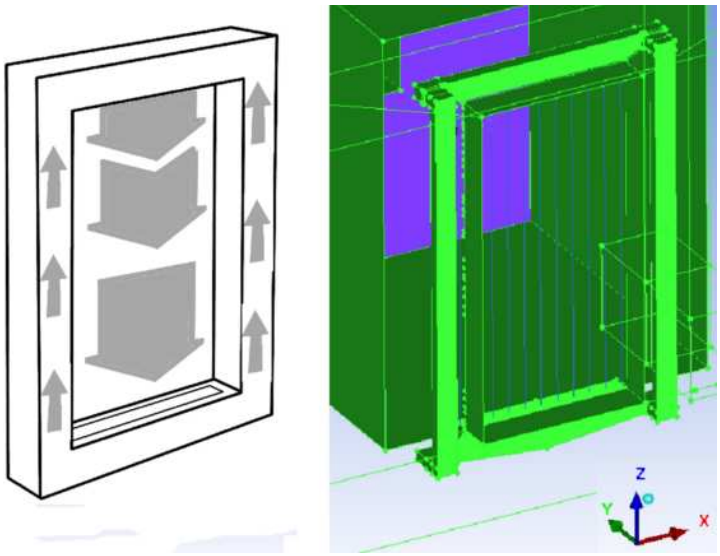

Figure 7: Geometry of the recirculating air curtain.

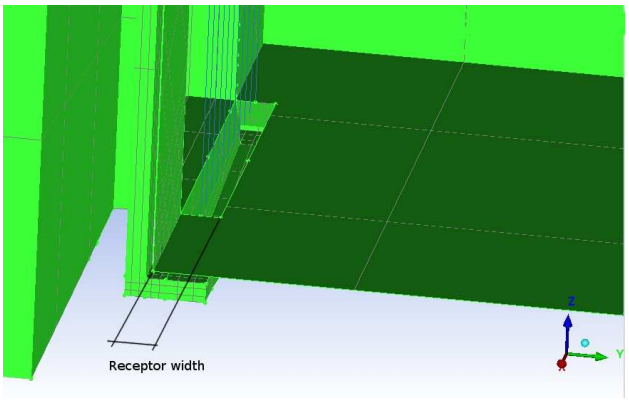

Figure 8: Detail of the recirculating ACU: receptor vent.

parametric study.

The region of the computational domain with the highest level of mesh concentration corresponds to the surroundings of the air curtain discharge, where the jet potential core region has been discretized with 35 layers of nodes in the streamwise direction (middle mesh). Regions far from the jet are not so critical and the mesh can therefore be less concentrated.

Computations have been carried out in a parallel high performance IBQDR cluster with 2304 cores. When 64 cores are used, the computational time is about 24 hours for the simulation of 10 seconds of the physical process.

4.2. Initial and boundary conditions

As initial conditions, t=0, the air has been assumed stagnant over the whole domain. The concentration of water vapour and temperatures are specified in both inner and outer spaces. For the inner refrigerated space, an initial temperature of 278 K and a humidity ratio of 0.005 g/kg of dry air (which corresponds to 90% of relative humidity) are given. The ambient or

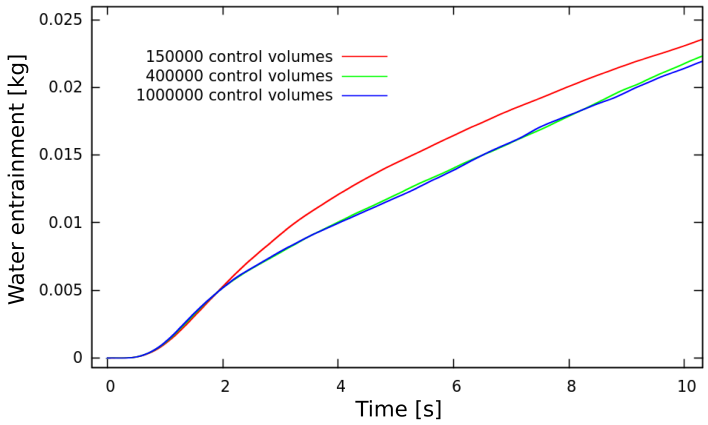

Figure 9: Comparison between three meshes with different concentrations.

outer space initial temperature and relative humidity are later specified for the different test cases. All the domain is considered at atmospheric pressure.

As was mentioned in the subsection 2.2, zero velocities are considered at the solid surfaces in both inner and outer spaces. Regarding the energy equation, solid surfaces are assumed adiabatic for the outer space and isothermal in the refrigerated room. The usual adiabatic condition considered by other authors has been substituted by a constant temperature condition (specifically, 281 K). This boundary condition allows to consider inertial effects, as it is detailed in the next subsection. At the ACU discharge section velocity and inclination angle are given. For the temperature and moisture level at this discharge, the upstream values, corresponding to the humid air of the refrigerated chamber at the entrance/suction of the ACU have been taken.

In the case of the recirculating device. the same treatment has been given for the ACU discharge. The receptor vent placed in the ground has a suction effect due to the connection with the ACU discharge section.

Finally, in the walls where condensation is produced an instantaneous drain of the liquid water is assumed.

4.2.1. Thermal inertia of the walls

Although the walls of a refrigerating chamber have been usually treated as adiabatic, in this study a fixed temperature is given in order to take into account their thermal inertia.

To demonstrate this, the unsteady behaviour of typical walls in refrigerated chambers has been analysed. The considered wall is 7 cm thick. It is composed by two thin metallic plates and a thick insulation material between them. Air is kept at 278 K in the inner space, while the temperature in the outer space is 298 K. Initially (t=0), the wall temperature distribution corresponds to the steady-state solution (linear profile). What happens when the temperature in the inner space changes? Specifically, the effect of a sudden increase of temperature in inner space (to 298 K) is here considered.

Temperature distribution in the wall along the time is given in Fig.10. As can be seen, the surface temperature remains near 281 K for more than a minute. In this period of time, the walls act as an energy sink, due to its low temperature. If an adiabatic boundary condition is assumed, this energy sink would not be taken into account.

Therefore, for this study a boundary condition with fixed temperature is considered more appropriate than the standard adiabatic condition.

4.3. Parametric studies

In this section, three parametric studies are presented. The main characteristics are summarized in Table 1, where the type of ACU (non-recirculating

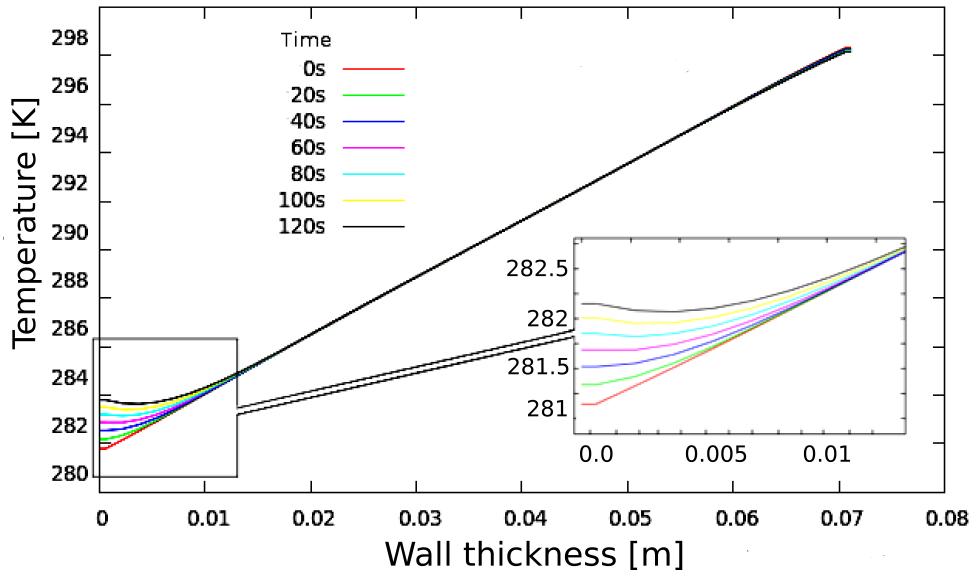

Figure 10: Time evolution of the transversal temperature profile inside the wall.

single jet, twin-jet and recirculating), discharge conditions (velocities and inclinations angles), and ambient values (relatve humidity and temperature) are specified.

In the first study, the thermal energy and moisture entrainment are studied considering different discharge conditions, but keeping ambient temperature and humidity. The condensation produced on the walls of the refrigerated room is also determined. In the second parametric study, the velocity and discharge angles have been fixed while humidity and temperature of the outer space (ambient) are changed. In the third study, non-recirculating (standard single jet), twin-jet and recirculating ACUs are compared, obtaining their efficiencies in the same scenario (discharge and ambient conditions).

Although experimental data on refrigerated chambers are not available to

compare the results, the previous validation studies indicate the capability of the employed model to produce a reliable description.

4.3.1. First parametric study: effect of the ACU discharge velocity and angle

This first parametric study is focused on the thermal energy entering a refrigerated chamber with a doorway sealed by the ACU. The modified input parameters are the discharge velocity and the discharge angle. As it is indicated in Table 1, different discharge velocities and discharge angles have been tested.

The thermal efficiency of the ACU can be defined as:

$$E_{ffQ} = 1 - \frac{Q_{on}}{Q_{off}} \tag{16}$$

where Q_{on} and Q_{off} are the thermal energy gains with the air curtain turned on and turned off, respectively. These energy gains are calculated integrating the inlet heat fluxes from the initial instant until the steady state is reached. Similarly, the mass entrainment efficiency can be defined as:

$$E_{ffM} = 1 - \frac{M_{on}}{M_{off}} \tag{17}$$

where M_{on} and M_{off} are the water mass entrainment with the air curtain turned on and turned off, respectively. Similarly to the energy gains, these quantities are integrated along the time.

The temperature distribution for the case of $5m/s$ and $10m/s$ are shown in Fig.11(a) and Fig.11(b) respectively.

As can be seen, a higher discharge velocity does not necessarily mean a higher sealing efficiency of the doorway. The case with the ACU operating

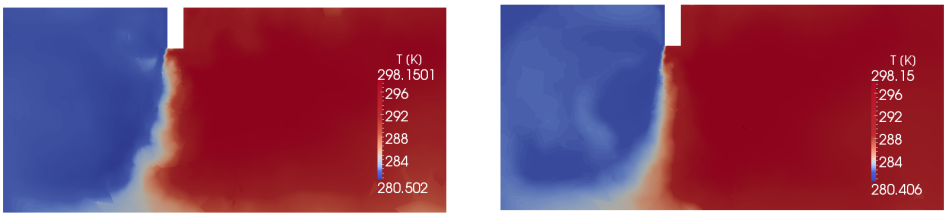

(a) (b)

Figure 11: Temperature distribution in the whole domain with two discharge velocities: (a) 5m/s; (b) 10m/s.

at $10m/s$ exhibits a refrigerated room with higher temperatures due to the higher external entrainment (Fig.11(b)). An analogue behaviour has been observed for the humid concentrations inside the refrigerated room.

The energy and mass entrainments for the different velocities and discharge angles can be seen in Table 2. The corresponding thermal energy and mass efficiencies are given in Fig.12 and 13 respectively.

As previously mentioned, a higher sealing efficiency is not necessarily obtained with a higher discharge velocity. This is due to the fact that excessive velocities enhance the mixing between the air in the outer and the air in the inner space. On the other hand, the lowest velocities will not produce an air jet strong enough to act as a separator with external forces deflecting it. A moderate discharge angle towards the outside increases the efficiency because it reduces that deflection. For this particular configuration, the optimum is found for the discharge velocity of 5.0 m/s with an angle of $-7.5°$ (the minus sign indicates towards the outer space) (see Fig.12).

The moisture penetrating through the doorway is convected in the refrig-

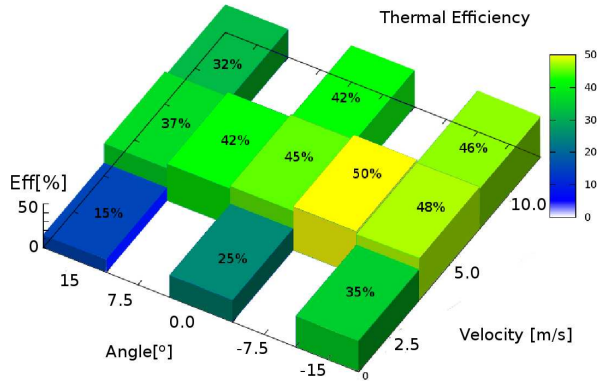

Figure 12: Thermal energy efficiency for each ACU discharge velocity and discharge angle.

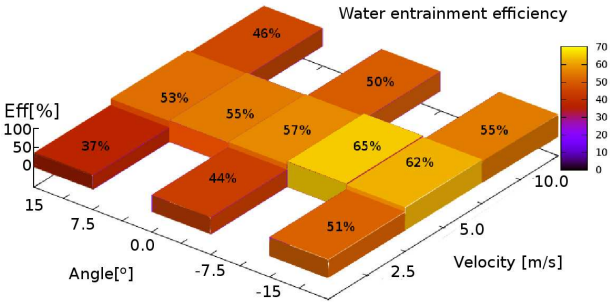

Figure 13: Water entrainment efficiency for each ACU discharge velocity and discharge angle.

erated space and diffuses to the cold walls. When the temperature of the wall is lower than the dew point temperature, the phenomenon of surface condensation occurs. The amount of condensed water per unit area on each of the surfaces during the first 20.0 seconds is given in Table 3.

As previously mentioned, the different discharge velocities are not equally effective for different times opening the door. It can be distiguished three stages. The initial instants when the air has not been accelerated enough by the stack effect (i.e. the force generated against the jet due to the difference of temperatures between inside and outside of the refrigerated space) defined the first stage. The ACU is not reducing the entrainment compared to the ACU when turned off. Once the air jet is completely developed, it produces the desired effect insulating the inner space. In the second stage the entrainment exhibit a pronounced increase because the ACU is not covering the whole doorway. It can even slightly accelerate the arrival of humid air to the room. In the third stage, the evolution acquires its steady state, because the inner space has reached the ambient temperature.

The discharge angle of the ACU has also been modified in order to determine the required position that produces the higher efficiency of the device. It can be seen that the best performance is obtained with negative discharge angles (towards the outside), according to the experience.

If the difference of pressure between the refrigerated chamber and the outer space increases or other forces (e.g. wind) were applied, higher angles than the ones indicated here could be required in order to compensate the deflection of the air jet.

4.3.2. Second study: Influence of ambient temperature and relative humidity

This section is focused on the effect of the temperature and moisture differences between the outer space and the refrigerated chamber.

The input parameters are the temperature and moisture at the outer space, mantaining the refrigerated chamber at 278 K. The discharge velocity is fixed at 5.0 m/s, and the discharge angle is 0°.

Fig.14(a) gives the time evolution of the thermal entrainment. It shows that the thermal entrainment is not highly affected by the variations of the moisture level in the outer space. This is a logical result, because the stack effect is due to the difference of density mainly produced by the difference of temperature between inside and outside.

Fig.14(b) gives the time evolution of the water vapour entrainment. It shows that the effect of modifying both the levels of moisture and temperature at the outer space clearly affects the amount of water vapour entering the refrigerated room, increasing the amount of water penetrating through the doorway as the temperature difference and/or the humidity difference increases.

The condensation on the surfaces of the refrigerated room can be seen in Fig.15 and 16. The effect of a higher temperature of the ambient increases the amount of condensation in the refrigerated chamber, with a higher amount of water collected on the walls and on the ground than on the ceiling. The same effect is observed for the ambient relative humidity. These results indicate that the ACU is partially preventing the thermal and mass entrainment, but not totally. As it has been pointed out in the previous section, in these studies only the stack effect is acting as external force. If any other external

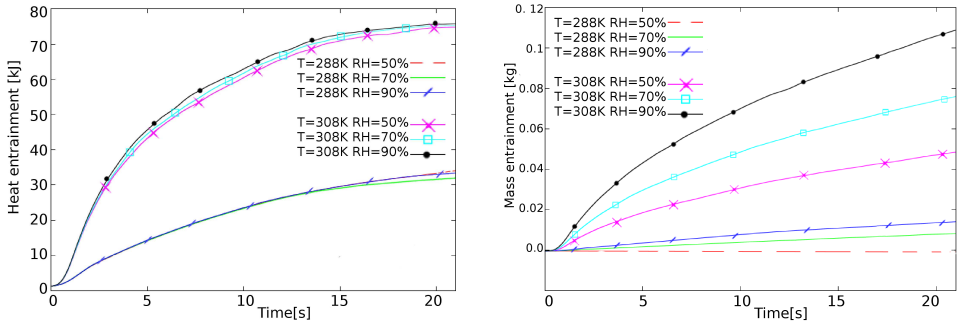

(a) (b)

Figure 14: Thermal entrainment (a) and mass entrainment (b) considering different ambient temperature and relative humidity.

force acts against the air jet, thermal and mass entrainments will increase.

4.3.3. Third parametric study: Comparison of different air curtain configurations

In this final section three different configurations are considered: non-recirculating single jet, twin-jet and recirculating ACU. The efficiency corresponding to the three different configurations is presented.

The first configuration is the non-recirculating single jet, which is the reference configuration employed in the previous sections. The second configuration is the non-recirculating twin-jets, which consists of a double jet with a 3 cm separation between them. The third configuration is the recirculating ACU, which is a more complex system. This system has ducts placed inside the walls to redirect the air jet collected in the receptor vent (see Fig.8) to the ACU suction/entrance section.

In this study, the discharge angle has been fixed in 0 degrees. The ob-

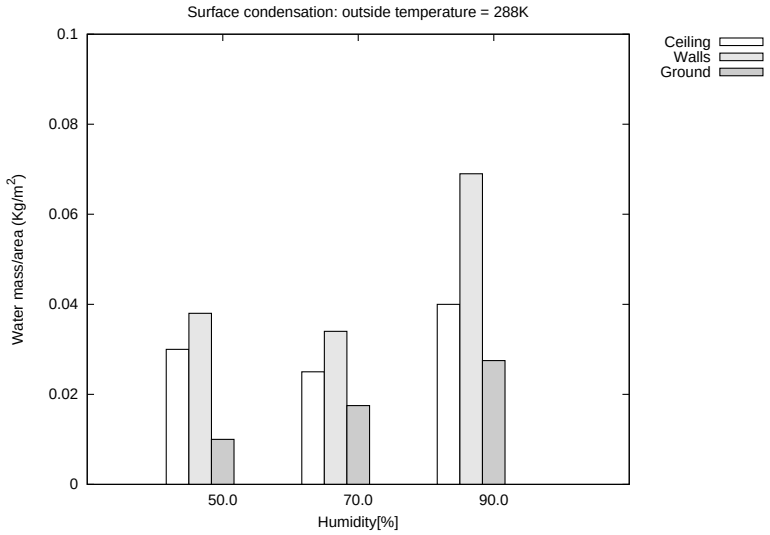

Figure 15: Surface condensation on the refrigerated space considering an ambient temperatures of 288 K.

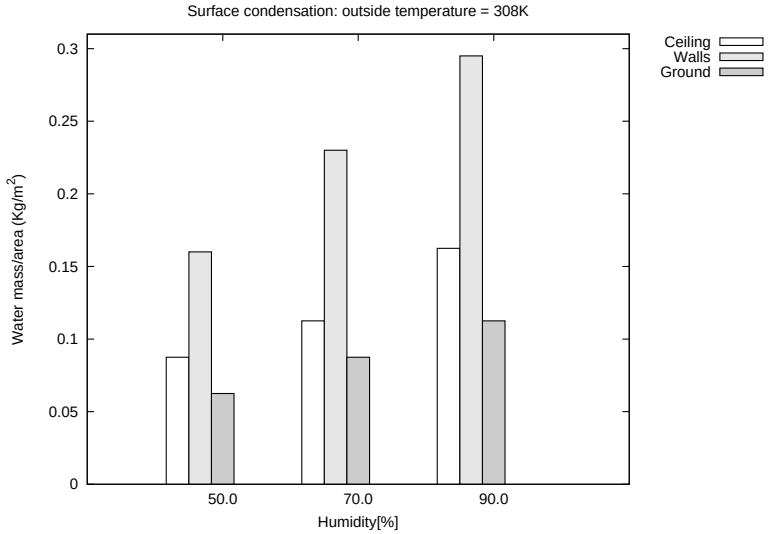

Figure 16: Surface condensation on the refrigerated space considering an ambient temperatures of 308 K.

tained results are summarised in Fig.17. The twin-jets improve the sealing capability of the ACU compared to the non-recirculating single jet. This is due to the additional protection that the external jet (the one in contact with the outer space) gives to the internal one. In this way, the curvature of the jet is lower than in the single jet. It is worth noticing that, far from the discharge, the two jets finally merge in a single air stream. This is due to the deformation of the rectangular jets as they advance: their shapes are progressively changed from rectangular to circular. Once this state is achieved, it is observed that the two jets are interacting between them.

At the initial simulation instants, when the air jets are not totally closing the door, the efficiency of the single and twin-jets is exactly the same (see Fig.18).

As mentioned above, the higher sealing capability is obtained with the recirculating system. Even when the installation of the recirculating ACU is more expensive than the non-recirculating one, the present results pointed out that this type of installation can produce an overall economic benefit. The receptor vent has a double effect: it diminishes the mixture of the inside/outside air and, moreover, diminishes the curvature of the jet due to the produced suction effect. This enhance in the jet stability was also pointed out by Valkeapää and Sirén [10]. They observed an increase in the ACU efficiency of 20% for the recirculating installation compared with the non-recirculating. In the present study an increase of 30-40% has been found. This discrepancy can be due to the different working conditions. It is worth mentioning that the receiver vent should be correctly placed and wide enough to circulate all the air stream of the jet.

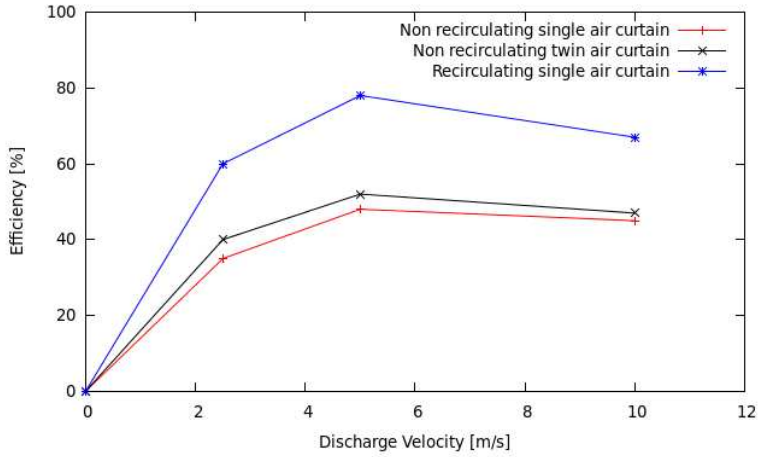

Figure 17: ACU thermal efficiency with different velocities and configurations: single jet, twin-jet and recirculating ACU.

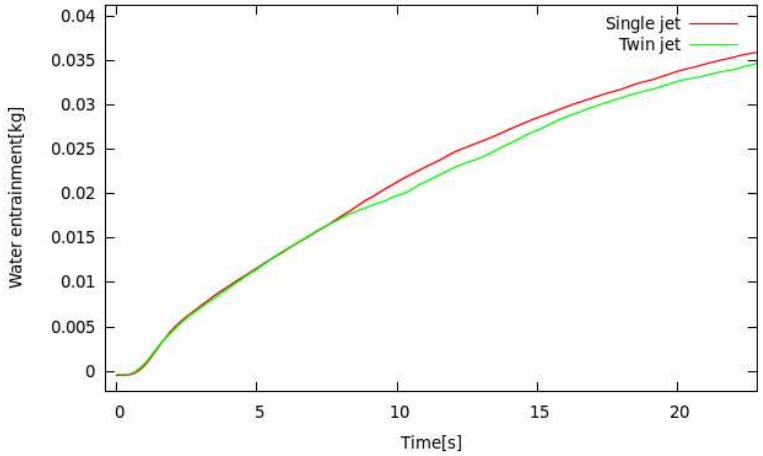

Figure 18: Temporal evolution of the mass entrainment: comparison between single jet and twin-jet. Discharge velocity fixed at 5m/s.

5. Conclusions

CFD calculations using LES modelling for the prediction of air curtain units (ACUs) efficiencies have been presented. The model considers the effect of both thermal energy and moisture entrainment through the protected opening. Furthermore, the influence of the water vapour distribution in the refrigerated space and possible condensation on the cold walls have also been taken into account.

The model has been validated by comparing the results with experimental measurements from the authors and from the literature. Special attention has been paid to the mass transfer effects.

The influence of the discharge velocities has been studied. Optimum values have been determined to minimize humidity and thermal energy entrainment through the doorway. Different discharge angles have been studied to determine the position that produces the highest efficiency. It has been observed that low discharge angles towards the outside of the chamber produce the best performance.

A detailed analysis of the three different configurations selected (single non-recirculating jet, twin-jets and single recirculating jet) has been carried out. In the case of twin-jets, a higher efficiency than the single jet configuration is observed. However, the highest efficiencies have been observed with the recirculating devices. The direct air recirculation system provides a maximum sealing performance of 80% for the optimum discharge velocity.

The main observations about the ACU discharge and configurations could be summarised as follows:

- Higher discharge velocities do not necessarily imply higher sealing effi-

ciency.

- A moderate discharge angle towards the outside increases the efficiency in refrigerated chambers.
- Twin-jets produce a moderate efficiency improvement compared to the single jet configuration.
- Recirculating air curtains produce a significant increase in the sealing efficiency compared to non-recirculating configurations.
- Thermal energy and mass entrainment are equally affected by the ACU discharge velocity and angle.

Acknowledgements

This work has been financially supported by the Ministerio de Economía y Competitividad, Secretaría de Estado de Investigación, Desarrollo e Innovación, Spain (Project VAPFLOW, ENE-2012-36910).

References

[1] G. Hetsroni and C. W. Hall. Further Studies of the Air Curtain. *ASAE Transactions*, 1:438–452, 1964.

[2] F. C. Hayes and W. F. Stoecker. Design Data for Air Curtains. *ASHRAE Transactions*, 2121:168–179, 1969.

[3] K. Sirén. Technical Dimensioning of a Vertically Upwards Blowing Air Curtain. Part I. *Energy and Buildings*, 35:681–695, 2003.

[4] K. Sirén. Thechnical Dimensioning of a Vertically Upwards Blowing Air Curtain-part II. *Energy and Buildings*, 35:697–705, 2003.

[5] H. Giráldez, C. D. Pérez-Segarra, I. Rodríguez, and A. Oliva. Improved semi-analytical method for air curtains prediction. *Energy and Buildings*, 60:256–266, 2013.

[6] A.M. Foster, M.J. Swain, R. Barrett, P. D'Agaro, S.J. James, Effectiveness and optimum jet velocity for a plane jet air curtain used to restrict cold room infiltration. *International Journal of Refrigeration*, Volume 29, Issue 5, 692–699,August 2006.

[7] A. M. Foster, M. J. Swain, R. Barrett, P. D'Agaro, L. Ketteringham, and S. J. James. Three-Dimensional Effects of an Air Curtain Used to Restrict Cold Room Infiltration. *Applied Mathematical Modelling*, 31(6):1109–1123, 2007.

[8] Paola D'Agaro, Giovanni Cortella, Giulio Croce. Two- and Three-dimensional CFD Applied to Vertical Display Cabinets Simulation. *International Journal of Refrigeration*, 29:178–190, 2005.

[9] Giovanni Cortella, Marco Manzan, Gianni Comini, CFD simulation of refrigerated display cabinets. *International Journal of Refrigeration*, Volume 24, Issue 3, 250–260, 2001.

[10] Valkeapää, A., Sirén, K. The influence of air circulation, jet discharge momentum flux and nozzle design parameters on the tightness of an upwards blowing air curtain *International Journal of Ventilation*, 8 (4): 337-346, 2010.

[11] E. Hammond, J. Quarini, A. Foster. Development of a stability model for a vertical single band recirculated air curtain sealing a refrigerated cavity. *International Journal of Refrigeration*, 34:1455-1461, 2011.

[12] Homayun K. Navaz, Brenda S. Henderson, Ramin Faramarzi, Ahmad Pourmovahed, Frederic Taugwalder. Jet entrainment rate in air curtain of open refrigerated display cases. *International Journal of Refrigeration*, Volume 28, Issue 2, 267–275, March 2005.

[13] Marinetti S., Cavazzini G., Lauri I., Testa S., Minetto S. Numerical and experimental analysis of the air flow distribution in the cooling duct of a display cabinet. *International Journal of Refrigeration*, 42: 8–13, 2014.

[14] J. E. Jaramillo, C. D. Pérez-Segarra, A. Oliva, and C. Oliet. Analysis of the Dynamic Behaviour of Refrigerated Space Using Air Curtains. *Numerical Heat Transfer, Part A*, 55(6):553–573, 2009.

[15] M. Tamm. Zur Berechnung von Luftschleiern,Dissertation. 1975.

[16] F. Nicoud and F. Ducros. Subgrid-scale stress modeling based on the square of the velocity gradient tensor. *Flow, Turbulence and Combustion*, 62:183–200, 1999.

[17] T. E. Fessler. Wetair - A Computer Code for Calculating Thermodynamic and Transport Properties of Air-Water Mixtures *Tech. Report 1466*, NASA, 1979.

[18] Launder Heat and Mass Transport in Turbulence. Chapter 6, Ed. Bradshaw, Springer, Berlin, (1978).

[19] Reynolds The prediction of turbulent Prandtl and Schmidt numbers. Int.J.Heat Mass Transfer, Vol.18, p1055, (1975).

[20] O. Lehmkuhl, C. D. Pérez-Segarra, R. Borrell, M. Soria, and A. Oliva. TERMOFLUIDS: A new Parallel unstructured CFD code for the simulation of turbulent industrial problems on low cost PC Cluster. In *Proceedings of the Parallel CFD 2007 Conference*, pages 1–8, 2007.

[21] R. W. C. P. Verstappen and A. E. P. Veldman. Symmetry-preserving discretization of turbulent flow. *Journal of Computational Physics*, 187(1):343–368, 2003.

[22] F. X. Trias and O. Lehmkuhl. A self-adaptive strategy for the time integration of Navier-Stokes equations. *Numerical Heat Transfer, Part B*, 60(2):116–134, 2011.

[23] I. Rodríguez, R. Borrell, O. Lehmkuhl, C. D. Perez-Segarra, and A. Oliva. Direct numerical simulation of the flow over a sphere at $Re = 3700$. *Journal of Fluid Mechanics*, 25(25):263–283, 2011.

[24] O. Lehmkuhl, I. Rodríguez, A. Baez, A. Oliva and C. D. Perez-Segarra. On the large-eddy simlulations for the flow around aerodynamic profiels using unstructured grids. *Computers & Fluids*, 80:176–189, 2013.

[25] D. Kizildag, F.X. Trias, I. Rodríguez, A. Oliva. Large eddy and direct numerical simulations of a turbulent water-filled differentially heated cavity of aspect ratio 5. *International Journal of Heat and Mass Transfer*, 77:1084–1094, 2014.

[26] Trias, F.X., Lehmkuhl, O., Oliva, A., Pérez-Segarra, C.D., Verstappen, R.W.C.P. Symmetry-preserving discretization of Navier-Stokes equations on collocated unstructured grids. *Journal of Computational Physics*, 258: 246–267, 2014.

[27] Air Movement and Control Association International. *ANSI/AMCA Standard 220-05. Laboratory Methods of Testing Air Curtain Units for Aerodynamic Performance Rating.*, 2005.

[28] H. Giráldez, C. D. Pérez-Segarra, I. Rodríguez, and A. Oliva. Optimization of the Thermal and Fluid Dynamic Behaviour of Air Curtains. Analysis of the Plenum by Means of LES. In *Proceedings of the 15th International Conference on Fluid Flow Technologies,Budapest,Hungary*, 2012.

[29] Talukdar, P., Iskra, C.R., Simonson, C.J. Combined heat and mass transfer for laminar flow of moist air in a 3D rectangular duct: CFD simulation and validation with experimental data. *International Journal of Heat and Mass Transfer*, 51(11-12):3091–3102. 2008.

[30] S. Ben Jabrallah, A.S. Cherif, B. Dhifaoui, A. Belghith, J.P. Corriou Experimental study of the evaporation of a falling film in a closed cavity. *Desalination*,180, Issues 1â3,197–206, 2005.

List of Figures

1 Case 1: Trajectories of air jets produced by an ACU. (a)Air jet which presents an excessive deflection due to external forces. (b)Air jet which totally seals a refrigerated chamber. 14

2 Case 2: Scheme of the horizontal pool case. 16
3 Case 2: Air flow film temperature and relative humidity at the duct outlet. Comparison of numerical results and experimental data (from [29]). 17
4 Case 3: Scheme of the falling film on a vertical wall. 18
5 Case 3: Falling film. Comparison of the numerical results and experimental data (from [30]). (a)Temperature distribution in the horizontal middle section (x, y=H/2, z=W/2). (b)Temperature distribution along the wall. 18
6 (a) Geometry of the calculation domain and (b) Detail of the computational mesh in the doorway. 21
7 Geometry of the recirculating air curtain. 21
8 Detail of the recirculating ACU: receptor vent. 22
9 Comparison between three meshes with different concentrations. 23
10 Time evolution of the transversal temperature profile inside the wall. 25
11 Temperature distribution in the whole domain with two discharge velocities: (a) 5m/s; (b) 10m/s. 27
12 Thermal energy efficiency for each ACU discharge velocity and discharge angle. 28
13 Water entrainment efficiency for each ACU discharge velocity and discharge angle. 28
14 Thermal entrainment (a) and mass entrainment (b) considering different ambient temperature and relative humidity. . . . 31

15 Surface condensation on the refrigerated space considering an ambient temperatures of 288 K. 32
16 Surface condensation on the refrigerated space considering an ambient temperatures of 308 K. 32
17 ACU thermal efficiency with different velocities and configurations: single jet, twin-jet and recirculating ACU. 34
18 Temporal evolution of the mass entrainment: comparison between single jet and twin-jet. Discharge velocity fixed at 5m/s. 34

Study	$v[m/s]$	$\theta[^\circ]$	$RH_{amb}[\%]$	$T_{amb}[K]$	$Type$
First	2.5	-15.0	90.0	298.0	Single jet
	2.5	0.0	90.0	298.0	Single jet
	2.5	15.0	90.0	298.0	Single jet
	5.0	-15.0	90.0	298.0	Single jet
	5.0	-7.5	90.0	298.0	Single jet
	5.0	0.0	90.0	298.0	Single jet
	5.0	7.5	90.0	298.0	Single jet
	5.0	15.0	90.0	298.0	Single jet
	10.0	-15.0	90.0	298.0	Single jet
	10.0	0.0	90.0	298.0	Single jet
	10.0	15.0	90.0	298.0	Single jet
Second	5.0	0.0	50.0	288.0	Single jet
	5.0	0.0	70.0	288.0	Single jet
	5.0	0.0	90.0	288.0	Single jet
	5.0	0.0	50.0	308.0	Single jet
	5.0	0.0	70.0	308.0	Single jet
	5.0	0.0	90.0	308.0	Single jet
Third	5.0	0.0	90.0	298.0	Single jet
	5.0	0.0	90.0	298.0	Twin-jet
	5.0	0.0	90.0	298.0	Recirculating

Table 1: Parametric studies conditions.

$v[m/s]$	$\theta[^\circ]$	$Heat[kJ]$	$Mass[kg]$
0.0	-	114	0.083
2.5	-15.0	77.52	0.045
2.5	0.0	66.12	0.041
2.5	15.0	61.56	0.037
5.0	-15.0	71.82	0.039
5.0	-7.5	66.12	0.037
5.0	0.0	62.7	0.035
5.0	7.5	57	0.029
5.0	15.0	59.28	0.031
10.0	-15.0	96.9	0.052
10.0	0.0	85.5	0.046
10.0	15.0	74.1	0.040

Table 2: Heat and mass entrainment considering different discharge angles and discharge velocities.

$v[m/s]$	$\theta[^\circ]$	Mass water/surface (kg/m^2)		
-	-	Ceiling	Walls	Ground
2.5	-15.0	0.0875	0.100	0.05
2.5	0.0	0.099	0.112	0.041
2.5	15.0	0.12	0.101	0.028
5.0	-15.0	0.055	0.058	0.043
5.0	-7.5	0.054	0.062	0.045
5.0	0.0	0.063	0.086	0.053
5.0	7.5	0.0676	0.085	0.047
5.0	15.0	0.058	0.082	0.043
7.5	-15.0	0.059	0.057	0.032
7.5	0.0	0.085	0.092	0.062
7.5	15.0	0.095	0.063	0.058

Table 3: Condensation on the different surfaces of the refrigerated chamber with different discharge angles.